HHS Public Access

Author manuscript

J Allergy Clin Immunol. Author manuscript; available in PMC 2020 January 01.

Published in final edited form as:

J Allergy Clin Immunol. 2019 January ; 143(1): 258–265. doi:10.1016/j.jaci.2018.06.012.

CVID patients with autoimmune cytopenias exhibit hyperplastic yet inefficient germinal center responses

Neil Romberg, MD[1,5,*], **Carole Le Coz, PhD**[1], **Salomé Glauzy, PhD**[8], **Jean-Nicolas Schickel, PhD**[8], **Melissa Trofa, BA**[1], **Brian E. Nolan, MD**[2], **Michele Paessler, DO**[3,6], **Mina LuQing Xu, MD**[9], **Michele Lambert, MD**[4,5], **Saquib A. Lakhani, MD**[10,13], **Mustafa K. Khokha, MD**[10,11,13], **Soma Jyonouchi, MD**[1,5], **Jennifer Heimall, MD**[1,5], **Patricia Takach, MD**[7], **Paul J. Maglione, MD, PhD**[14], **Jason Catanzaro, MD**[10], **F. Ida Hsu, MD**[12], **Kathleen E. Sullivan, MD PhD**[1,5], **Charlotte Cunningham-Rundles, MD, PhD**[14], and **Eric Meffre, PhD**[8,12,*]

[1]Division of Immunology and Allergy, The Children's Hospital of Philadelphia

[2]Division of Rheumatology, The Children's Hospital of Philadelphia

[3]Division of Hematopathology, The Children's Hospital of Philadelphia

[4]Division of Hematology, The Children's Hospital of Philadelphia

[5]Department of Pediatrics, The Perelman School of Medicine at the University of Pennsylvania, Philadelphia, Pennsylvania, USA

[6]Department of Pathology and Laboratory Medicine, The Perelman School of Medicine at the University of Pennsylvania, Philadelphia, Pennsylvania, USA

[7]Department of Medicine, Section of Allergy and Immunology, The Perelman School of Medicine at the University of Pennsylvania, Philadelphia, Pennsylvania, USA

[8]Department of Immunobiology, Yale University School of Medicine, New Haven, Connecticut, USA

[9]Department of Pathology, Yale University School of Medicine, New Haven, Connecticut, USA

[10]Department of Pediatrics, Yale University School of Medicine, New Haven, Connecticut, USA

[11]Department of Genetics, Yale University School of Medicine, New Haven, Connecticut, USA

[12]Department of Medicine, Yale University School of Medicine, New Haven, Connecticut, USA

[*]corresponding authors: Eric Meffre, PhD, Yale University School of Medicine, 300 George Street, Room 353F, New Haven, CT06511, USA, Phone: 203-737-4535, eric.meffre@yale.edu, Neil Romberg, MD, The Children's Hospital of Philadelphia, Abramson Research Center, Room 1216C, Philadelphia, PA 19104, USA, Phone: (267) 426-2836, rombergn@email.chop.edu.

Author contributions: NR, CLC, MT, JNS, SG, BN performed experiments and analyzed data. MP, MLX and NR performed histological analyses. KES, PJM, CCR, JC, FIH, SJ, ML, JH, ML, PT and NR provided patient samples. MKK and SL genotyped subjects. EM and NR were responsible for study design and wrote the manuscript. All authors reviewed the manuscript and provided scientific input.

Conflict of Interest Disclosure Statement: The authors have no financial conflicts of interest to disclose.

[13]Department of Pediatric Genomics Discovery Program, Yale University School of Medicine, New Haven, Connecticut, USA

[14]Division of Clinical Immunology, Department of Medicine, Icahn School of Medicine at Mount Sinai, New York, NY, USA

Abstract

Background: The lack of pathogen-protective, isotype-switched antibodies in common variable immunodeficiency (CVID) suggests germinal center hypoplasia, yet a subset of CVID patients is paradoxically affected by autoantibody-mediated autoimmune cytopenias (AICs) and lymphadenopathy.

Objective: We sought to compare the physical characteristics and immunological output of germinal center responses in CVID patients with AICs (CVID+AIC) and without AICs (CVID-AICs).

Methods: We analyzed germinal center size and shape in excisional lymph node biopsies from 14 CVID+AIC and 4 CVID-AIC patients. Using paired peripheral blood samples, we determined how AICs specifically impacted B and T cell compartments and antibody responses in CVID patients.

Results: We found that CVID+AIC patients displayed irregularly-shaped, hyperplastic germinal centers (GCs), whereas GCs were scarce and small in CVID-AIC patients. GC hyperplasia was also evidenced by an increase in circulating T follicular helper cells, which correlated with decreased regulatory T cell frequencies and function. In addition, CVID+AIC patients showed serum endotoxemia associated with a dearth of isotype-switched memory B cells that displayed significantly lower somatic hypermutation frequencies than CVID-AIC counterparts. Moreover, IgG+ B cells from CVID+AIC patients expressed VH4-34 antibodies with unmutated AVY and NHS motifs which recognize both erythrocyte I/i self-antigens and commensal bacteria.

Conclusions: CVID patients with autoimmune cytopenias fail to contain mucosal microbiota and exhibit hyperplastic yet inefficient germinal center responses that favor the production of untolerized IgG+ B cell clones that recognize both commensal bacteria and hematopoietic I/i self-antigens.

Capsule Summary:

Common variable immunodeficiency patients with autoimmune cytopenias exhibit hyperplastic germinal center reactions that fail to generate isotype-switched, somatically- mutated, immune-protective antibodies and instead produce poorly mutated, non-tolerized antibodies that recognize commensal bacteria and hematopoietic self-antigens.

Keywords

common variable immunodeficiency; autoimmune cytopenias; germinal center responses; somatic hypermutation; B-cell tolerance; commensal bacteria; follicular helper T cell; regulatory T cell

INTRODUCTION

High-affinity antibodies of specific isotypes are essential protections against a vast diversity of pathogens. Antigen-specific responses often involve the generation of germinal centers (GCs) within secondary lymphoid tissues that create a unique environment where B cells expressing the highest affinity B-cell receptors (BCRs) capture native antigens from follicular dendritic cells (FDC) and present them to cognate T follicular helper (Tfh) cells (1,2). Subsequent B-cell proliferation occurs with simultaneous expression of activation-induced cytidine deaminase (AID), which mediates somatic hypermutation (SHM) and class-switch recombination (CSR), leading to affinity-matured isotype-switched antibodies and class-switched memory B cells. Immunocompromised AID-deficient mice and humans fail to generate mutated, high-affinity antibodies and exhibit hyperplastic GCs, increased frequencies of circulating Tfh (cTfh) cells and systemic cytokines that may interfere with tolerance and promote autoantibody production (3,4). It remains to be determined if similar GC physiopathology may apply to other primary immunodeficiencies.

Common variable immunodeficiency (CVID) encompasses a heterogeneous group of primary antibody deficiency disorders (5). CVID patients display decreased serum antibody concentrations, poorly protective vaccine titers and low isotype-switched B-cell frequencies (5,6). Paradoxically, autoantibodies, including self-reactive IgGs, can be detected in the plasma of CVID patients (7), and approximately 20% experience autoimmune cytopenias (CVID+AIC) mediated by autoantibodies targeting either erythrocytes (autoimmune hemolytic anemia; AIHA) or platelets (immune thrombocytopenia; ITP) or both (Evans syndrome) (5). It is unknown why some CVID patients generate autoantibodies to hematopoietic self-antigens whereas others do not (CVID-AIC) and if this could be related to alterations in GC responses.

We report that excisional lymph node biopsies from CVID+AIC patients display irregularly-shaped and hyperplastic GCs, whereas GC structures are scarce, small and circular in CVID-AIC patients. Despite large GCs, CVID+AIC patients harbor fewer isotype-switched B cells with poorly mutated IgG transcripts enriched in autoreactive *VH4-34* clones that also recognize commensal bacteria (8), thereby suggesting that CVID-associated autoimmunity may be triggered by failed containment of mucosal microbiota.

METHODS

Patients.

We obtained peripheral blood samples from 44 CVID patients with and without AICs (see Table E1 in this article's Online Repository at www.jacionline.org). Each patient met 1999 PAGID CVID diagnostic criteria and was receiving antibody replacement therapy, but not immune suppressive medications at the time of enrollment. The average age of enrolled CVID+AIC patients was 37.1 years old (range 7-68 years); 48% were male. The average age of enrolled CVID-AIC patients was 38.5 years old (range 10-67 years); 35% were male. For purposes of comparison, we also obtained peripheral blood samples from 12 immune competent patients with ITP. The group's average age was 19.9 years (range 8-42 years); 40% were male. We also obtained plasma samples from 6 AID-deficient patients (average

age 30.4 years (range 4-60 years), 50% male). We also analyzed peripheral blood samples from 43 related and unrelated HDs with a mean age of 37.2 years (range 8-59); 41.6% were male.

Patient excisional lymph node biopsy specimens were identified by review of our CVID cohort's medical records. 14 of 18 patients carried a CVID diagnosis at the time of node removal. Lymph nodes from five patients (1 CVID+AIC, 4 CVID-AIC) were obtained during breast or thyroid cancer staging prior to initiation of chemotherapy. All analyzed staging nodes were determined to be malignancy free by a clinical pathologist. We obtained paired node and blood samples from 14 CVID patients. In all cases, nodes excision preceded blood sample donation. The mean duration between excision and phlebotomy was 51.9 months (range: 3 months to 14 years). In addition, lymph nodes were obtained from four patients who did not donate blood samples. One was an autopsy specimen and another was excised from a patient before hematopoietic stem cell transplantation. Two patients did not consent to phlebotomy. Age-matched control and bacterial lymphadenitis lymph nodes were identified from available clinical pathology cases at Yale New Haven Hospital and the Children's Hospital of Philadelphia. Study protocols were approved by the institutional review boards of Yale University, Mount Sinai, the Children's Hospital of Philadelphia and the University of Pennsylvania.

Cell staining and sorting, cDNA, RT-PCR and VHsequence analyses.

Mononuclear cells were isolated from peripheral blood using ficoll density gradient centrifugation, and B cells were enriched using CD20 microbeads (Miltenyi Biotech). B cells were stained with anti-human CD19-Pacific Blue, anti-human CD27-PerCPCy5.5, anti-human CD21-APC and anti-human IgG-PE (all from Biolegend). Single $CD19^+CD21^+CD27^+IgG^+$ B cells from 12 CVID patients and 12 healthy donors were sorted on FACSAria (Becton Dickinson) or MoFlo Astrios EQ (Beckman Coulter) flow cytometers into 96-well PCR plates that were immediately frozen on dry ice. RNA from single cells was reverse-transcribed in the original 96 well plate in 12.5 μL reactions containing Superscript IIRT (Gibco BRL) for 45 minutes at 42°C. RT-PCR reactions, including primer sequences, were as described. In brief, IgG gene transcripts were amplified in 96-well plates with two rounds of nested PCRs using HotStar® Taq DNA polymerase (Qiagen) and 3.5 μL of cDNA as template for the first PCR reactions and 3.5 μL of PCR1 reaction as template for the second PCR reactions (9). *VH* sequences were analyzed using the National Center for Biotechnology Information (NCBI) IGBLAST software, and *VH4-34* transcripts were aligned to the germ-line consensus *VH4-34*01* sequence. We especially focused our analysis on the mutational status of the VH4-34 FWR1 Ala-Val-Tyr (AVY) motif responsible for I/i self-antigen binding and the Asn-His-Ser (NHS) motif in the CDR2 region that modulates antibody affinity to cognate antigens (8).

Lymph node staining and analysis.

Hematoxylin and eosin stained lymph node sections were analyzed at low-power (12.5X) on a DM4000B microscope (Leica Biosystems), to capture the nodes entire two-dimensional area with a Spot RT/SE Slider camera (Spot Imaging). Follicular structures were traced and scored for circularity *in silico* with ImageJ software (NIH freeware) using the formula:

$$\text{circularity} = 4\pi(\text{area}/\text{perimeter}^2)$$

Lymph node follicular composition was determined by dividing the combined 2-dimensional areas of all follicular structures by the total lymph node area excluding adipose rich or acellular fibrous tissues. All pathology images were reviewed by one or more hematopathologists. Immunohistochemical staining was performed with anti-CD21 (1:100, Dako), anti-CD3 (pre-diluted, Ventana), anti-CD20 (1:200, Dako) and anti-BCL6 (1:50, Dako) antibodies.

In vitro Treg suppression assay.

$CD4^+$ T cells were enriched using the EasySep® Human $CD4^+$ T cell enrichment kit (STEMCELL) or MojoSort™ Human CD4 T Cell Isolation Kit (Biolegend). $CD4^+CD25^{hi}CD127^{lo/-}$ Tregs and $CD3^+CD4^+CD25^-$ Tresp cells were sorted by flow cytometry and labeled with carboxyfluorescein diacetate succinimidyl ester (CFSE) (Thermo Fischer). Treg and Tresp cells were co-cultured at a 1:1 ratio with beads loaded with anti-CD2, anti-CD3 and anti-CD28 (Treg suppression inspector human, Miltenyi). Co-cultures were stained for viability with the LIVE/DEAD kit (Thermo Fisher), and proliferation of viable Tresp cells analyzed for CFSE dilution at 3.5-4.5 days.

Flow cytometry.

The following antibodies were used for flow cytometric stainings: anti-CD19 APC-Cy7, anti-CD27 PerCP-Cy5.5, anti-CD21 Pacific Blue, anti-CD4 APC-Cy7, anti-CD25 PE- Cy7, PE or PE Dazzle, anti-CD127 PerCP-Cy5.5 or APC, anti-CD45RO AF-700, anti-CXCR5 Pacific Blue, anti-PD-1 PE-Cy7 (all from BioLegend), anti-CD3 eFluor 605NC (eBioscience) and anti-IgG APC (Becton Dickinson). Intracellular staining with anti-Foxp3 Alexa Fluor 488 (eBioscience) or APC (Biolegend) was performed using the Foxp3/ Transcription Factor Staining Buffer Set (eBioscience) in accordance with manufacturer instructions.

Endotoxin quantification.

Endotoxin concentrations were determined in plasma samples using the Pierce™ LAL chromogenic endotoxin quantification kit (Thermo Fischer).

Statistics.

Data were analyzed with GraphPad Prism using either Mann-Whitney U tests or linear regression analysis.

RESULTS

IgA deficiency and endotoxemia correlate with AIC development in CVID patients.

To determine what humoral alterations promote CVID+AIC, we analyzed peripheral B cells from 26 CVID+AIC patients and compared them with counterparts from 18 age-matched CVID- AIC patients and 43 healthy donor (HD) controls. The CVID+AIC group included 8 patients with Evans Syndrome, 2 with AIHA and 16 with ITP whereas 8 of 18 CVID-AIC patients experienced other non-cytopenic inflammatory diseases (Table E1). The majority of

enrolled CVID patients lacked a molecular diagnosis although some pathologic mutations in CVID- associated genes including *CTLA4, NFKB1* and *TNFRSF13B* were identified mostly within the CVID+AIC group (Table E1). Our CVID+AIC cohort displayed increased frequencies of $CD19^{hi}CD21^{-/lo}$ B cells compared to CVID-AIC patients (25.0% vs. 3.8%, P<0.0001; Fig E1). This B cell subset, reported hyporesponsive *in vitro,* is enriched in autoreactive clones and predicts the development of autoimmune cytopenias and splenomegaly in "group Ia" CVID, a patient subset defined by the Freiburg classification criteria (6,10,11). In addition, we found more severely decreased $CD27^{+}IgG^{+}$ memory B-cell frequencies in CVID+AIC patients (on average 0.6% of total B cells) compared to CVID-AIC patients (2.8%) and HDs (5.4%, P<0.01 and P<0.0001, respectively; Fig 1, A and B). IgA^{+} B cells were also consistently scarce in CVID+AIC patients averaging only 0.3% of total B cells (P<0.0001 vs. control), whereas CVID- AIC patients displayed average frequencies similar to age-matched controls (3.4% vs. 4.4%, Fig 1, A and B).

CVID+AIC patients were uniformly IgA deficient, with an average serum concentration of 4.8 mg/dL, whereas the average concentration in CVID-AIC patients was significantly higher (50.8 mg/dL, P<0.001; Fig 1C). Since IgA antibodies contain commensal microbiota within the intestinal lumen and at other mucosal sites (12), we tested if CVID+AIC patients with the lowest serum IgA concentrations and circulating IgA^{+} memory B cell frequencies displayed bacterial endotoxins in their blood. Indeed, we found significantly elevated endotoxin concentrations in the plasma of CVID+AIC patients, which averaged 482 EU/μL and showed a concentration range similar to those in AID deficient patients with undetectable serum IgA. CVID-AIC patients displayed endotoxin levels similar to HDs (198 EU/μL vs 133 EU/μL; Fig 1D). We conclude that scarce IgA^{+} B cells, low serum IgA concentrations and endotoxemia specifically correlate with AIC development in CVID patients.

CVID+AIC patient IgG^{+} B cells express non-tolerized VH4-34 antibodies reported to recognize the hematopoietic I/i self-antigen and commensal bacteria

Since CVID+AIC patients displayed severely decreased class-switched memory B cells and resembled patients deficient for AID, which mediates CSR and SHM, we analyzed SHM frequencies in single IgG+ B cells isolated from six CVID+AIC patients, six CVID-AIC patients and twelve age-matched HDs (see Tables E2-E15). As previously reported by others, we found that CVID patients generally displayed lower SHM frequencies in heavy chain variable regions *(VH)* than controls (Fig 2A) (13,14). IgG *VH* transcripts from CVID +AIC patients showed the least SHM both when averaged by subject and in pooled sequences with an average of only 7.5 mutations per *VH* segment compared to 15.1 mutations for CVID-AIC patients and 18.6 mutations for HDs (CVID+AIC vs. CVID-AIC, P<0.0001; CVID+AICs vs. HD, p<0.0001; Fig 2A).

We also analyzed our cohort's IgG^{+} B-cell *VH* repertoires and found *VH3* gene segments to be most utilized followed by *VH4* segments with a *VH3:VH4* usage ratio of 2.5:1 in both HD and CVID-AIC groups (Fig 2B) (8,15). In contrast, CVID+AIC IgG^{+} B cells favored *VH4* gene segment usage with a *VH3:VH4* ratio of 1:1 (Fig 2B). This difference was driven by increased usage of the *VH4-34* gene segment identified in 9.9% of CVID+AIC *IgG*

transcripts, whereas *VH4-34* gene segments were rarely found in HD and CVID-AIC counterparts (Fig 2C and Fig E2) (8). VH4-34-encoded antibodies are intrinsically autoreactive and bind the conserved I/i carbohydrate self-antigen expressed by erythrocytes and other hematopoietic cells; self-antigen recognition relies on the Ala-Val-Tyr (AVY) motif in their framework region 1 (FWR1) independently of IgH complementarity determining region 3 (CDR3) and associated light chains (16-18). A second VH4-34 motif, a Asn-X-Ser (NHS) located in CDR2, modulates antibody/antigen avidity (18). *VH4-34*-encoded IgG antibodies also often recognize commensal bacteria when AVY and NHS motifs are unmutated (8). To determine how SHM differentially modifies these motifs in HD versus CVID+AIC patients, we aligned *VH4-34 IgG* transcripts with the germline consensus *VH4-34*01* sequence (Fig 2D). While HD *VH4-34* IgG transcripts displayed non-synonymous mutations in 64.6% of AVY motifs and 76.4% of NHS motifs, we identified these mutations in only 14.2% of AVY motifs and 28.4% of NHS motifs in VH4-34-expressing B cells from CVID+AIC patients who therefore appear to have undergone systemic IgG responses targeting mucosal microbiota (Fig 2, D and E). Hence, AIC development correlates with the presence of VH4-34-expressing IgG^+ B cells with unmutated AVY and NSH motifs that likely recognize both I/i self-antigen and translocated commensal bacteria.

Hyperplastic and irregularly-shaped germinal center responses specifically correlate with CVID+AIC patients

AID deficiency-associated loss of SHM results in hyperplastic GC responses due to sustained antigenic B-cell activation in the absence of competitive, mutated, high-affinity antibodies (3,4). To determine if severely decreased SHM in CVID+AIC patients impact their GC responses, we visualized GCs *in situ* through analysis of rare excisional lymph node biopsies from 18 CVID patients, 14 of whom donated blood samples for memory B cell analyses. In total, 24 malignancy-free CVID lymph nodes, which were removed to evaluate lymphadenopathy or for cancer staging prior to chemotherapy, were analyzed. For comparison, we also obtained malignancy-free control axillary lymph nodes from four immunocompetent patients (28-43 years). Hematoxylin and eosin-stained control lymph nodes displayed distinct and well-spaced GCs comprising approximately 5% (range 1.6-9.5%) of a node's cellular area (Fig 3, A and B). These structures were scarcer in CVID-AIC nodes occupying only 2% of the surface area (range 0.2%−1.9%, $P<0.01$; Fig 3, A and B, and Fig E3). In contrast, CVID+AIC GCs were hyperplastic covering on average 32.9% (range 18.5-44.4%) of node area ($P<0.001$; Fig 3, A and B, and Fig E4). In addition, *in silico* 2-dimensional scoring of control node GC shape generated an average circularity quotient (CQ) of 0.92 (range 0.87-0.98) while a perfect circle would generate a CQ of 1 (Fig 3C). CVID-AIC nodes also displayed circular-shaped GCs (average CQ 0.91, range 0.88- 0.96), whereas irregularly-shaped GCs were common in CVID+AIC nodes as illustrated by their reduced CQ score (0.67, range 0.09-0.9, $P<0.0001$ for both comparisons; Fig 3C). Many CVID+AIC GCs formed highly complex shapes potentially suggesting coalescence of multiple GC reactions, yet immunohistochemical stainings of these structures for CD20, CD3, BCL6 and CD21 suggested conventional GC cellular organization (Fig E5). Despite differences in age, lymph nodes from CVID+AIC children (n=1, 7 years old) and CVID

+AIC adolescents (n=2, 14 and 15 years old) appeared histologically similar to adult CVID +AIC patient nodes and quite dissimilar from age-matched control nodes.

Since GCs enlarge in response to infection, we also obtained three reactive lymph nodes from immunocompetent patients with cervical or axillary bacterial lymphadenitis (BL) to compare with CVID+AIC lymph nodes. Indeed, BL resulted in numerous, larger GCs comprising a greater average percentage of node cross-sectional area than GCs in control nodes (19.6% versus 5%, $P<0.05$; Fig E6, A and B). However, unlike many CVID+AIC GCs, these structures remained uniformly circular (average CQ score 0.94, range 0.86-0.97; Fig E6, C). We conclude that CVID+AIC patients display hyperplastic GCs with irregular shapes inconsistent with typical lymphadenitis, whereas CVID-AIC patients demonstrate weak follicular responses.

Expanded cTfh cells combined with a dearth of Tregs predict follicular hyperplasia and AICs in CVID patients

Hyperplastic GC reactions in AID-deficient patients correlate with increased $CD4^+CXCR5^+PD\text{-}1^{hi}$ cTfh cells that normally promote B-cell survival, proliferation and SHM (3). We previously reported that CVID patients with heterozygous *TNFRSF13B* mutations and many with AICs displayed increased cTfh frequencies, but we did not assess if this feature was associated with AICs or dysregulated GC reactions (7,19). We therefore compared cTfh frequencies in CVID+AIC and CVID-AIC patients, immune competent ITP patients and HDs. We found cTfh frequencies were significantly elevated in CVID+AIC patients (range 10.2%−32.9%) compared to those in CVID-AIC, ITP patients without CVID and HDs (1.3%−9.6%, $P<0.0001$; Fig 4, A and B). In addition, while regulatory T cells (Tregs) represented around 5% of the HD and ITP patient $CD4^+$ T compartments, Treg frequencies were significantly decreased in CVID patients, especially with AICs (Fig 4B). Bivariate analysis of cTfh and Treg frequencies from HDs, immune competent ITP patients and CVID patients revealed an inverse and linear relationship between these variables ($R^2=0.31$, $p<0.0001$), with values assigned to CVID+AIC patients forming a unique cluster defined by cTfh abundance and Treg paucity (Fig 4C). Moreover, $CVID^+AIC$ $CD4^+CD25^{hi}CD127^{lo}$ Tregs failed to suppress the *in vitro* proliferation of HD T- responder cells (Tresp), whereas CVID-AIC Tregs displayed intermediate suppressive capacities (Fig 4, D and E). Thus, AIC development in CVID correlates with an expanded cTfh cell compartment combined with quantitative and qualitative Treg alterations.

DISCUSSION

Altogether, we show here that AIC development in CVID patients is associated with hyperplastic and irregularly-shaped GCs, which correlate with reduced IgA, endotoxemia, elevated cTfh frequencies, Treg dearth, and severely reduced isotype-switched memory B cell compartments containing decreased SHM and enriched in non-tolerized autoreactive VH4-34-expressing IgG^+ clones. Several of these features were previously identified in AID-deficient patients and in CVID patients with lymphadenopathy/tonsillar hyperplasia and are likely linked to altered SHM (3,7,20,21). Abrogated and decreased SHM due to either inborn AID deficiency or poor AID induction previously described in CVID B cells

(22), respectively, diminishes generation of high-affinity antibodies that normally constrain GC reactions by either competing with GC B cells for binding sites on specific FDC-provided antigens and/or by forming inhibitory immune- complexes that co-crosslink BCRs and inhibitory FcγRIIb receptors (2,3,23). Hence, prolonged B-cell activation when SHM is either impaired or decreased likely favors Tfh expansion and secretion of IL-4, IL-21 and inflammatory cytokines that may alter Treg function (3,7).

Decreased SHM combined with defective CSR also limits anti-commensal IgA production that may result in failed mucosal microbiota containment, especially in the gut, further inducing systemic immune responses involving GCs (8). In agreement with this hypothesis, high plasma levels of endotoxins were previously reported in CVID patients prior IgG replacement therapy (24). Among our IgG replete cohort, we found increased bacterial endotoxin plasma concentrations specifically in IgA-deficient CVID+AIC patients who also possessed VH4- $34^{+}IgG^{+}$ B cells with unmutated AVY and NHS motifs that have recently been reported to recognize commensal bacteria (8). Since these AVY- and NHS-unmutated VH4-34^{+} IgG clones are also autoreactive and recognize the I/i self-antigens expressed on the surface of erythrocytes and other hematopoietic cells types (16-18), we propose that these antibodies may contribute to the destruction of red blood cells in CVID patients with hemolytic anemia and perhaps platelets in those with thrombocytopenia, thereby potentially mediating AICs.

Supplementary Material

Refer to Web version on PubMed Central for supplementary material.

Acknowledgments:

We are very much indebted to the patients. We thank Drs. L. Devine, F. Tuluc and C. Wang for cell sorting.

Funding: This work was supported by grant number K23AI115001 from National Institutes of Health-National Institute of Allergy and Infectious Diseases (NIH-NIAID), the Jeffrey Modell Foundation (to N.R.), and AI-061093, AI-071087 and AI-082713 from NIH-NIAID (to E.M.).

Abbreviations:

AIC	autoimmune cytopenias
AID	activation-induced cytidine deaminase
AIHA	autoimmune hemolytic anemia
APC	allophycocyanin
BCR	B-cell receptor
BL	bacterial lymphadenitis
CDR3	complementarity determining region 3
CFSE	carboxyfluorescein diacetate succinimidyl ester

CSR	class-switch recombination
CVID	common variable immunodeficiency
FDC	follicular dendritic cell
FWR	framework region
GC	germinal center
HD	healthy donor
PE	phycoerythrin
ITP	immune thrombocytopenia
SHM	somatic hypermutation
Tfh	follicular helper T cell
Treg	regulatory T cell
Tresp	responder T cell
VH	Heavy chain variable region

REFERENCES

1. Victora GD, Nussenzweig MC. Germinal centers. Annu Rev Immunol. 2012;30:429–57. [PubMed: 22224772]
2. Zhang Y, Meyer-Hermann M, George LA, Figge MT, Khan M, Goodall M, et al. Germinal center B cells govern their own fate via antibody feedback. J Exp Med. 2013 3 11;210(3):457–64. [PubMed: 23420879]
3. Cantaert T, Schickel J-N, Bannock JM, Ng Y-S, Massad C, Delmotte FR, et al. Decreased somatic hypermutation induces an impaired peripheral B cell tolerance checkpoint. J Clin Invest. 2016 11 1;126(11):4289. [PubMed: 27701145]
4. Zaheen A, Boulianne B, Parsa J-Y, Ramachandran S, Gommerman JL, Martin A. AID constrains germinal center size by rendering B cells susceptible to apoptosis. Blood. 2009 7 16;114(3):547–54. [PubMed: 19478044]
5. Bonilla FA, Barlan I, Chapel H, Costa-Carvalho BT, Cunningham-Rundles C, de la Morena MT, et al. International Consensus Document (ICON): Common Variable Immunodeficiency Disorders. J Allergy Clin Immunol Pract. 2016 2;4(1):38–59. [PubMed: 26563668]
6. Warnatz K, Denz A, Drager R, Braun M, Groth C, Wolff-Vorbeck G, et al. Severe deficiency of switched memory B cells (CD27+IgM-IgD-) in subgroups of patients with common variable immunodeficiency: a new approach to classify a heterogeneous disease. Blood. 2002 3 1;99(5): 1544–51. [PubMed: 11861266]
7. Romberg N, Chamberlain N, Saadoun D, Gentile M, Kinnunen T, Ng YS, et al. CVID- associated TACI mutations affect autoreactive B cell selection and activation. J Clin Invest. 2013 10 1;123(10): 4283–93. [PubMed: 24051380]
8. Schickel J-N, Glauzy S, Ng Y-S, Chamberlain N, Massad C, Isnardi I, et al. Self-reactive VH4-34-expressing IgG B cells recognize commensal bacteria. J Exp Med. 2017 7 3;214(7):1991–2003. [PubMed: 28500047]
9. Wardemann H, Yurasov S, Schaefer A, Young JW, Meffre E, Nussenzweig MC. Predominant autoantibody production by early human B cell precursors. Science. 2003 9 5;301(5638):1374–7. [PubMed: 12920303]

10. Isnardi I, Ng Y-S, Menard L, Meyers G, Saadoun D, Srdanovic I, et al. Complement receptor 2/CD21- human naive B cells contain mostly autoreactive unresponsive clones. Blood. 2010 6 17;115(24):5026–36. [PubMed: 20231422]

11. Rakhmanov M, Keller B, Gutenberger S, Foerster C, Hoenig M, Driessen G, et al. Circulating CD21low B cells in common variable immunodeficiency resemble tissue homing, innate-like B cells. Proc Natl Acad Sci. 2009 8 11;106(32): 13451—6. [PubMed: 19666505]

12. Johansen FE, Pekna M, Norderhaug IN, Haneberg B, Hietala MA, Krajci P. Absence of epithelial immunoglobulin A transport, with increased mucosal leakiness, in polymeric immunoglobulin receptor/secretory component-deficient mice. J Exp Med. 1999 10 4;190(7):915–22. [PubMed: 10510081]

13. Almejun MB, Campos BC, Patino V, Galicchio M, Zelazko M, Oleastro M, et al. Noninfectious complications in patients with pediatric-onset common variable immunodeficiency correlated with defects in somatic hypermutation but not in class-switch recombination. J Allergy Clin Immunol. 2017 3;139(3):913–22. [PubMed: 27713077]

14. Levy Y, Gupta N, Le Deist F, Garcia C, Fischer A, Weill J- C, et al. Defect in IgV gene somatic hypermutation in Common Variable Immuno-Deficiency syndrome. Proc Natl Acad Sci U S A. 1998 10 27;95(22):13135–40. [PubMed: 9789054]

15. Roskin KM, Simchoni N, Liu Y, Lee J-Y, Seo K, Hoh RA, et al. IgH sequences in common variable immune deficiency reveal altered B cell development and selection. Sci Transl Med. 2015 8 26;7(302)

16. Potter KN, Hobby P, Klijn S, Stevenson FK, Sutton BJ. Evidence for involvement of a hydrophobic patch in framework region 1 of human V4-34-encoded Igs in recognition of the red blood cell I antigen. J Immunol Baltim Md 1950. 2002 10 1;169(7):3777–82.

17. Reed JH, Jackson J, Christ D, Goodnow CC. Clonal redemption of autoantibodies by somatic hypermutation away from self-reactivity during human immunization. J Exp Med. 2016 6 27;213(7):1255–65. [PubMed: 27298445]

18. Sabouri Z, Schofield P, Horikawa K, Spierings E, Kipling D, Randall KL, et al. Redemption of autoantibodies on anergic B cells by variable-region glycosylation and mutation away from self-reactivity. Proc Natl Acad Sci U S A. 2014 6 24; 111(25):E2567–2575. [PubMed: 24821781]

19. Morita R, Schmitt N, Bentebibel S-E, Ranganathan R, Bourdery L, Zurawski G, et al. Human blood CXCR5(+)CD4(+) T cells are counterparts of T follicular cells and contain specific subsets that differentially support antibody secretion. Immunity. 2011 1 28;34(1):108–21. [PubMed: 21215658]

20. Unger S, Seidl M, Schmitt-Graeff A, Bohm J, Schrenk K, Wehr C, et al. Ill-defined germinal centers and severely reduced plasma cells are histological hallmarks of lymphadenopathy in patients with common variable immunodeficiency. J Clin Immunol. 2014 8;34(6):615–26. [PubMed: 24789743]

21. Lougaris V, Faletra F, Lanzi G, Vozzi D, Marcuzzi A, Valencic E, et al. Altered germinal center reaction and abnormal B cell peripheral maturation in PI3KR1-mutated patients presenting with HIGM-like phenotype. Clin Immunol. 2015 7 1; 159(1):33–6. [PubMed: 25939554]

22. : Yu JE, Knight AK, Radigan L, Marron TU, Zhang L, Sanchez-Ramon S. Toll-like receptor 7 and 9 defects in common variable immunodeficiency. J Allergy Clin Immunol. 2009 8;124(2):349–56. [PubMed: 19592080]

23. Nimmerjahn F, Ravetch JV. Fcgamma receptors as regulators of immune responses. Nat Rev Immunol. 2008 1;8(1):34–47. [PubMed: 18064051]

24. Perreau M, Vigano S, Bellanger F, Pellaton C, Buss G, Comte D, et al. Exhaustion of bacteria-specific CD4 T cells and microbial translocation in common variable immunodeficiency disorders. J Exp Med. 2014 9 22;211(10):2033–45. [PubMed: 25225461]

Key Messages

- CVID patients with autoimmune cytopenias exhibit enlarged and irregularly shaped germinal centers whereas CVID patients without autoimmune cytopenias demonstrate hypoplastic germinal centers.
- Despite follicular hyperplasia, CVID patients with autoimmune cytopenias generate few isotype-switched B cells with low frequency of somatic hypermutations.
- An IgA deficiency-associated failure to contain mucosal microbiota may generate systemic immune responses in CVID patients with autoimmune cytopenias favoring the production of non-tolewrized *VH4-34-expressing* IgG + B cells recognizing both commensals and hematopoietic I/i self-antigens.

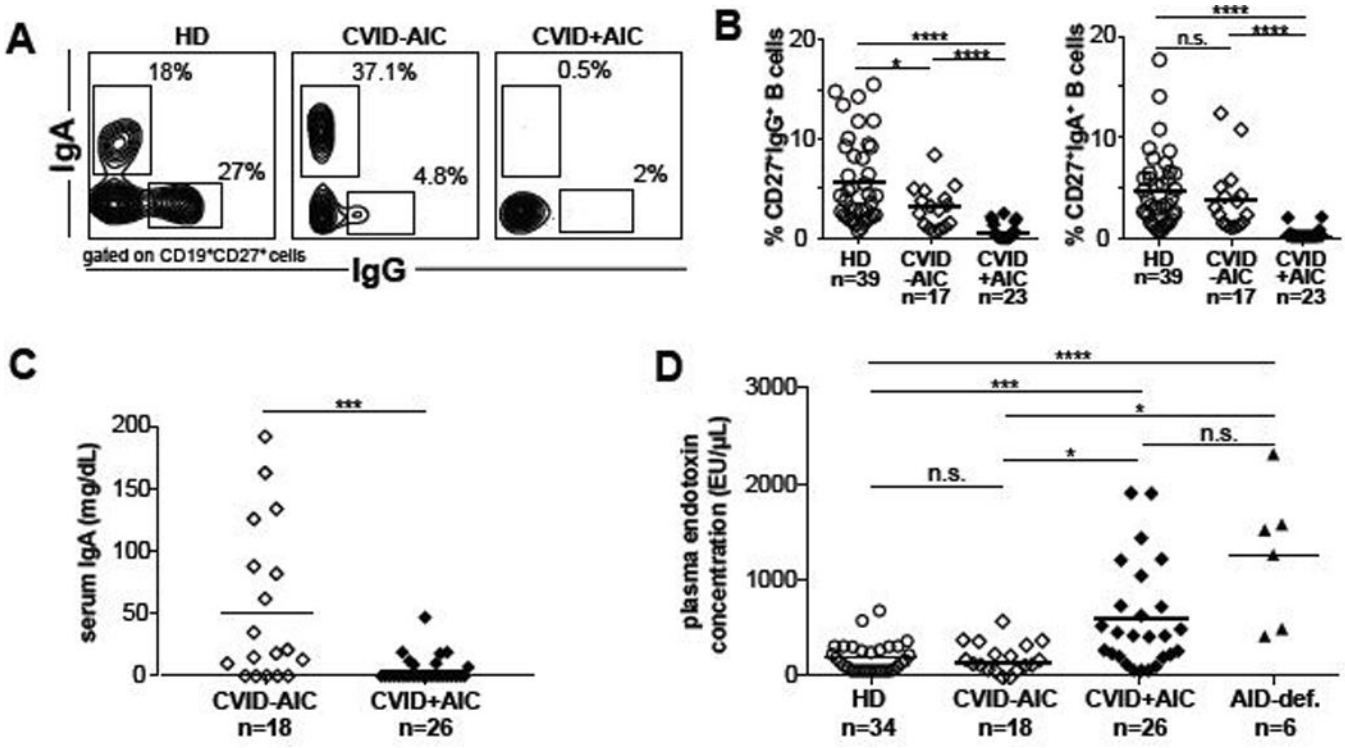

FIG 1. IgA deficiency and elevated plasma endotoxin concentrations correlate with AIC development in CVID patients.

Representative dot plots of IgG and IgA expression on $CD19^{+}CD27^{+}$ gated memory B cells from the indicated subjects are shown in (A). (B) $CD27^{+}IgG^{+}$ and $CD27^{+}IgA^{+}$ B cell frequencies in HD and CVID patients without or with AIC displayed as proportions of total circulating B cells. (C) Serum IgA and (D) plasma endotoxin concentrations are displayed. Dark bars represent average group values. Statistically significant differences are indicated, **P <0.01, ****P <0.0001 (Mann-Whitney U tests).

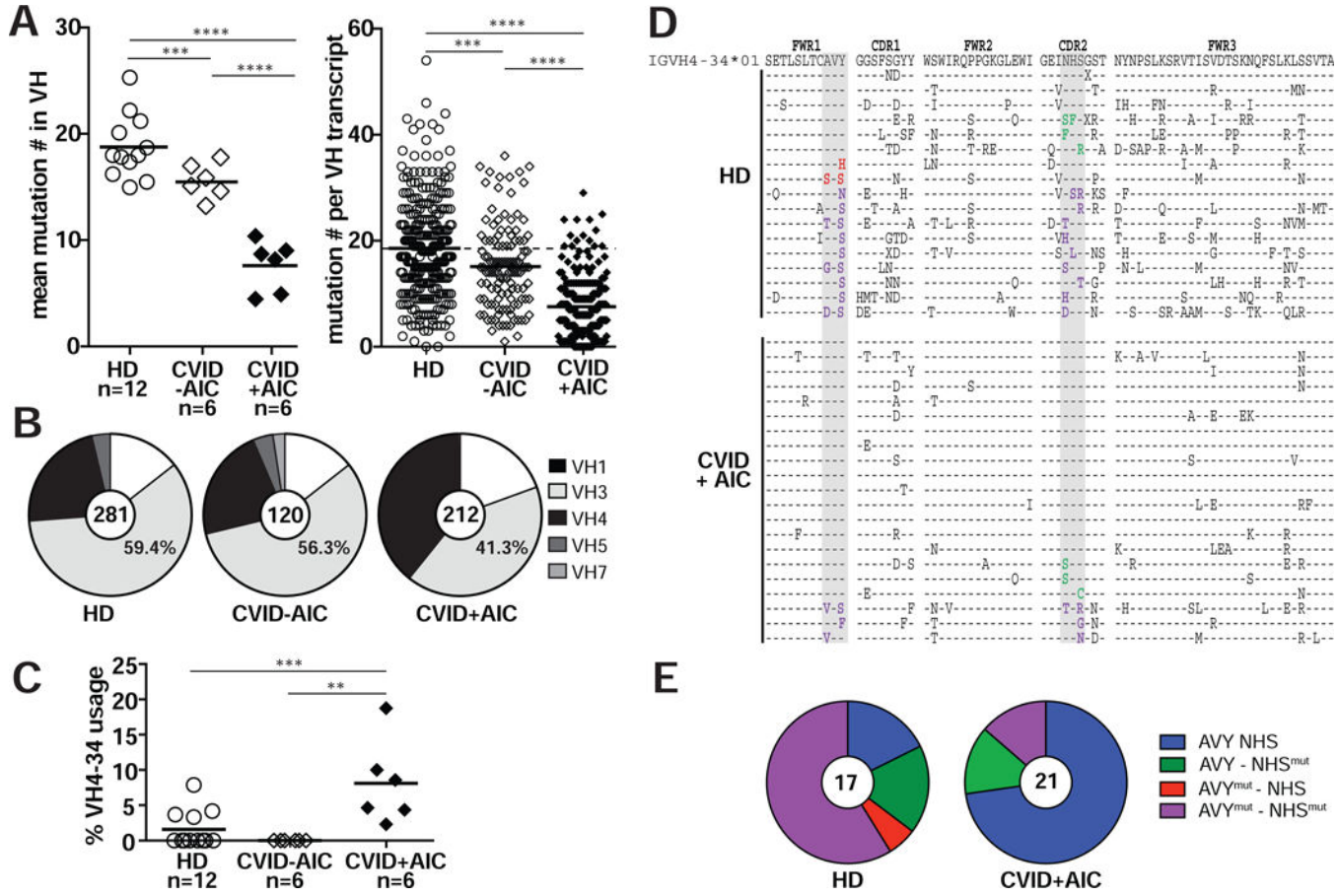

FIG 2. IgG$^+$ B cells from CVID+AIC patients display low SHM frequencies and an altered *VH* repertoire.

(A) Mutations in *VH* transcripts from CD27$^+$IgG$^+$ B cells from 12 healthy donors (HDs, open circles), 6 CVID patients without AICs (CVID-AIC, open diamonds) and 6 CVID +AIC patients (black diamonds) are displayed as averaged mutation number per subject (left) and absolute mutation number per transcript (right). Black bars represent mean values. (B) Pie charts represent *VH family* gene segment usage from pooled *IgG* transcripts. Transcript numbers per group are indicated in each pie's center. (C) Averages of *VH4-34* gene segment usage in IgG$^+$ B cells. (D) VH4-34 amino acid sequence alignment for IgG$^+$ memory B cells from HDs and CVID+AIC patients relative to germline *IGHV4-34*01* (top). Identity to germline is denoted by a dash and substituted residues are indicated in black unless within the critical AVY or NHS motifs (gray columns) where text color is red or green, respectively. Substitutions within both motifs are indicated in purple. (E) Pie charts represent proportions of pooled transcripts in HDs and CVID+AIC patients with AVY and/or NHS substitutions. Statistically significant differences are indicated: **** P <0.0001, *** P <0.001, ** P <0.01 (Mann-Whitney U tests).

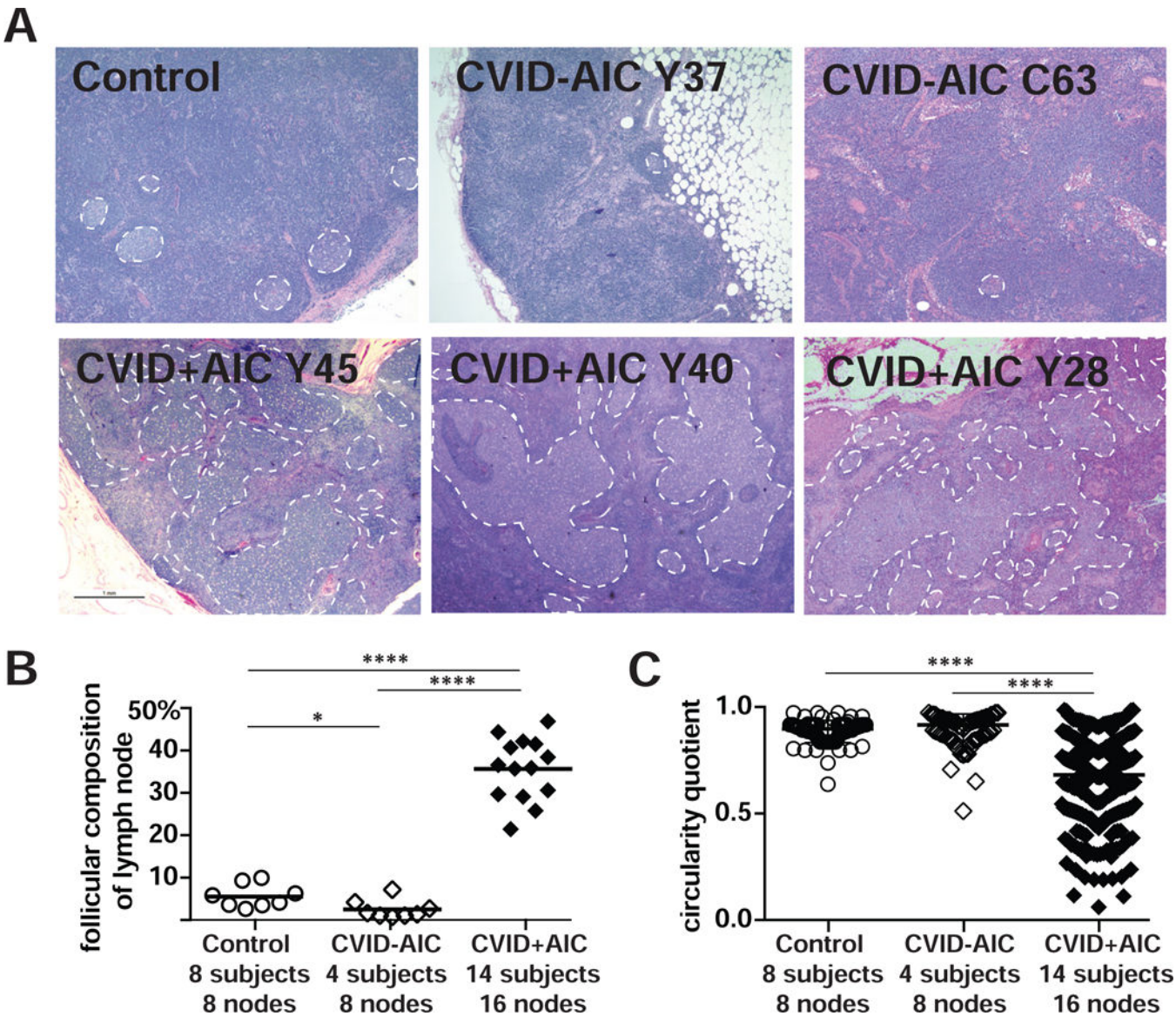

FIG 3. Asymmetric enlarged germinal centers (GCs) predominate in lymph nodes from CVID +AIC patients.

(A) Hematoxylin- and eosin-stained axillary lymph node biopsies from a representative immunocompetent 43-year-old female (Control), two CVID-AIC patients, and three CVID +AIC patients. GCs are outlined with white dashed lines. Original magnification, 12.5X. (B) The percentages of each lymph node's cellular two-dimensional surface comprised by GCs and (C) each GCs circularity quotient are represented for controls and patients. Statistically significant differences are indicated: ****P <0.0001, **P <0.01 (Mann-Whitney U tests).

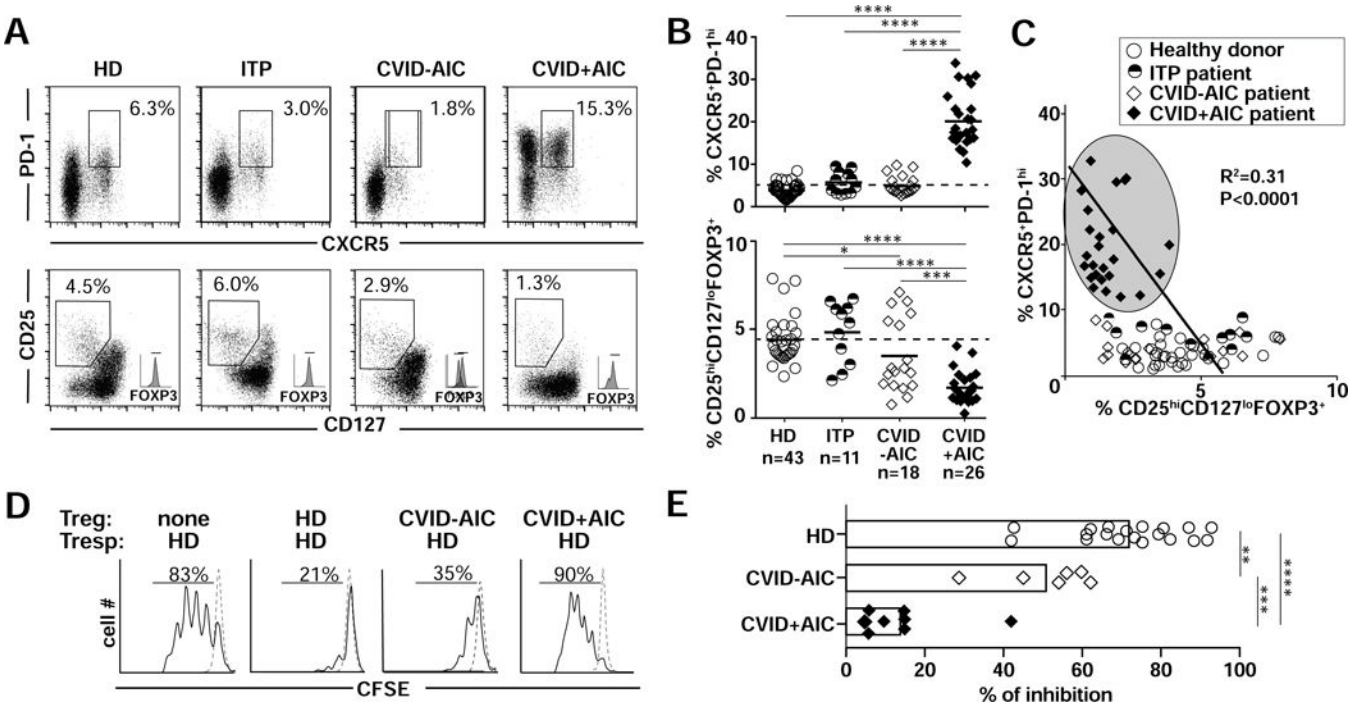

FIG 4. CVID+AIC patients show expanded cTfh and decreased Treg compartments.

(A) Dot plots show (top) CXCR5/PD-1 and (bottom) CD127/CD25 expression on gated $CD4^+$ T cells from representative HD, ITP, CVID-AID and CVID+AIC patients. (B) Summarized frequencies of $CD4^+CXCR5^+PD\text{-}1^{hi}$ cTfh and $CD4^+CD25^{hi}CD\ 127^{lo}FOXP3^+$ Treg in HD and patients. Black bars indicate averages. (C) Bivariate analysis of paired cTfh and Treg frequencies reveal that CVID+AIC patients segregate in a specific cTfh-rich and Treg-poor area (gray oval). (D) Representative histograms of heterologous CFSE-labeled HD T responder cell (Tresp) proliferation on day 4 co-cultured or not with $CD4^+CD25^{hi}CD127^{lo}$ Tregs from representative subjects. Dashed lines show unstimulated Tresp. (E) Summarized percentages of inhibition by Tregs from 19 HDs, 7 CVID-AICs patients and 7 CVID+AIC patients are represented. Statistically significant differences are indicated: ****P<0.0001, ***P<0.001, **P<0.01 (Mann-Whitney U tests or linear regression analysis).